AFCRL-63-131

Technical Report 75

ONE-SIDED MULTIPACTOR DISCHARGE MODES

Prepared for:

AIR FORCE CAMBRIDGE RESEARCH LABORATORIES
OFFICE OF AEROSPACE RESEARCH
UNITED STATES AIR FORCE
BEDFORD, MASSACHUSETTS

CONTRACT AF 19(628)-32
PROJECT 4600
TASK 460001

By *I. T. Vance* *J. E. Nanevicz*

Requests for additional copies by Agencies of the Department of Defense, their contractors, and other Government agencies should be directed to the:

DEFENSE DOCUMENTATION CENTER (DDC)
ARLINGTON HALL STATION
ARLINGTON 12, VIRGINIA

Department of Defense contractors must be established for DDC services or have their 'need-to-know' certified by the cognizant military agency of their project or contract.

All other persons and organizations should apply to the:

U.S. DEPARTMENT OF COMMERCE
OFFICE OF TECHNICAL SERVICES
WASHINGTON 25, D.C.

STANFORD RESEARCH INSTITUTE
MENLO PARK, CALIFORNIA

April 1963

AFCRL-63-131

Technical Report 75

ONE-SIDED MULTIPACTOR DISCHARGE MODES

Prepared for:

AIR FORCE CAMBRIDGE RESEARCH LABORATORIES
OFFICE OF AEROSPACE RESEARCH
UNITED STATES AIR FORCE
BEDFORD, MASSACHUSETTS

CONTRACT AF 19(628)-325
PROJECT 4600
TASK 460001

By: E. F. Vance J. E. Nanevicz

SRI Project No. 3977

Approved:

T. Morita

T. MORITA, MANAGER ELECTROMAGNETIC SCIENCES LABORATORY

D. R. Scheuch

D. R. SCHEUCH, DIRECTOR ELECTRONICS AND RADIO SCIENCES DIVISION

Copy No. 33

ABSTRACT

Modes of multipactor discharge occurring in a biased gap are described in which secondary emission from only one electrode is required to sustain the discharge. An analysis of these modes and an experimental corroboration of the theory are presented. It is shown that the lower threshold voltages for the mode in which only one electrode participates are generally lower than for the modes in which both electrodes participate. The application of a dc bias to a multipactor gap may therefore lower the RF voltage at which breakdown occurs.

FOREWORD

This report represents a continuation of work done under earlier Air Force contracts. The first 74 reports in this series are listed at the end of this report, under their appropriate contract numbers.

CONTENTS

ILLUSTRATIONS

I INTRODUCTION

Under high vacuum, where electron mean free path is comparable to or greater than electrode spacing, RF discharges may occur in which the electrons emitted at one electrode are accelerated across the gap in one half-cycle and impact with sufficient energy to produce at least one electron by secondary emission. The secondary electrons are accelerated back across the gap during the next half-cycle, again producing secondary electrons on impact. When the number of secondary electrons produced is greater than the number of incident electrons, the number of electrons participating increases until limits imposed by diffusion losses and space-charge distortion of the RF field are reached. This discharge process has been investigated by von Engel et al.,[1,2*] Hatch and Williams,[3,4] and others.

The biased multipactor discharge, in which a dc voltage, in addition to the RF voltage, is applied across the gap, has been investigated by Bol[5] and Milazzo.[6] In both of the investigations, however, consideration was given only to those modes in which the electron crossed the gap and collided with the opposite electrode. In the lowest mode considered, the electron crosses the gap against the dc field in somewhat greater than one-half of the RF cycle and the secondary electrons it produces cross the gap in the opposite direction (with the dc field) in somewhat less than one-half cycle, so that the total transit time to the electrode and back corresponds to one RF cycle. Higher-order modes in which the total transit time corresponds to integer multiples of RF cycles have been postulated.

Another multipactor mode in which the electrons are acted on by an RF electric field and a static magnetic field has been described by Brown.[7] In this mode, the electron is pulled away from the emitting electrode by the RF field, but because of the transverse magnetic field, the trajectory is curved. With the proper electric and magnetic field strengths, the trajectory will be such that the electron returns to the

*References are listed at the end of this report.

electrode at the end of the second RF cycle with sufficient energy to produce secondary emission. The discharge thus occurs near one electrode.

Until recently, interest in the multipactor discharge has been limited since the required electrode spacing, mean free path, and frequency are generally found only in microwave vacuum tubes such as klystrons, etc. With the increased emphasis on satellite-to-earth and satellite-to-satellite communication systems in recent years, however, the multipactor discharge has become a potential source of trouble in many areas outside the microwave tube field. Antennas, antenna couplers, RF connectors, and other RF equipment may be subject to multipactor discharges under the high-vacuum condition existing at satellite altitudes. Mean free paths at these altitudes are sufficiently great that multipactor discharges are not limited to microwave frequencies, but may occur at HF or lower if electrode spacings are appropriate. It appeared conceivable that certain irregularities in the signal from the earlier Sputniks might be the result of multipactor discharges occurring at the antenna or some other part of the RF system. Discussions with satellite experimenters indicated that they were probably experiencing multipactor breakdowns in their RF equipment including connectors and cavities. A study of the multipactor discharge was therefore initiated in which, among other things, the effect of dc bias between the electrodes was determined experimentally at frequencies of 30 to 40 megacycles per second.

During these experiments with biased multipactor discharges, an anomaly was observed in the relation between RF breakdown voltage and dc bias voltage which could not be accounted for by the theory developed by Bol[5] or Milazzo.[6]

A typical example of this anomaly is shown in Fig. 1, where experimental data taken with copper parallel-plate electrodes at 34.8 megacycles are compared with the RF threshold voltages predicted by Milazzo's analysis. As can be seen, the experimental data display a definite minimum in the lower breakdown curve, while the theoretical lower breakdown curve increases monotonically with increasing bias voltage. Although

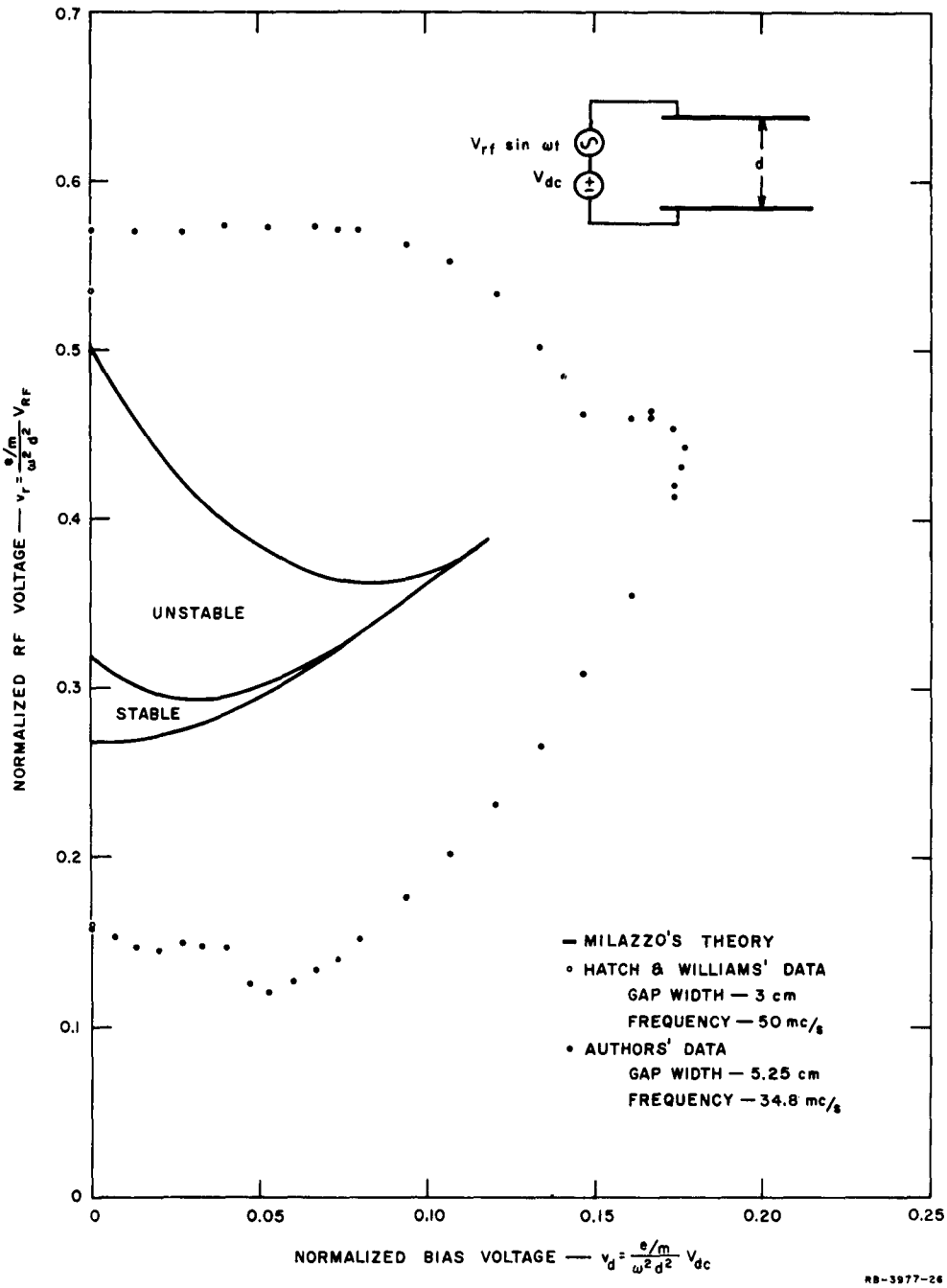

FIG. 1 THEORETICAL AND EXPERIMENTAL REGIONS OF BIASED MULTIPACTOR DISCHARGE

Milazzo's analysis was quite idealized, it did not seem probable that the observed minimum could be attributed to any of the assumptions made in his analysis. It was found that the anomaly could be explained, however, if a new, one-sided mode of multipactor discharge were postulated. The purpose of this report is to present an analysis and experimental verification of the one-sided modes. Consideration of the general problem of RF breakdown at satellite altitudes will be reserved for a later report.

In the one-sided mode, which can occur in the presence of dc fields, the electrons emitted from the positive electrode are pulled away from the electrode (against the dc field) by the RF field during most of the first half cycle. As the net field (dc plus RF) reverses, the electrons are pulled back toward the electrode. For the proper frequency and field strength, the electrons return to the emitting electrode at the end of one RF cycle with sufficient energy to produce secondary emission. Figure 2 illustrates the field strength and electron velocity and displacement as functions of time.

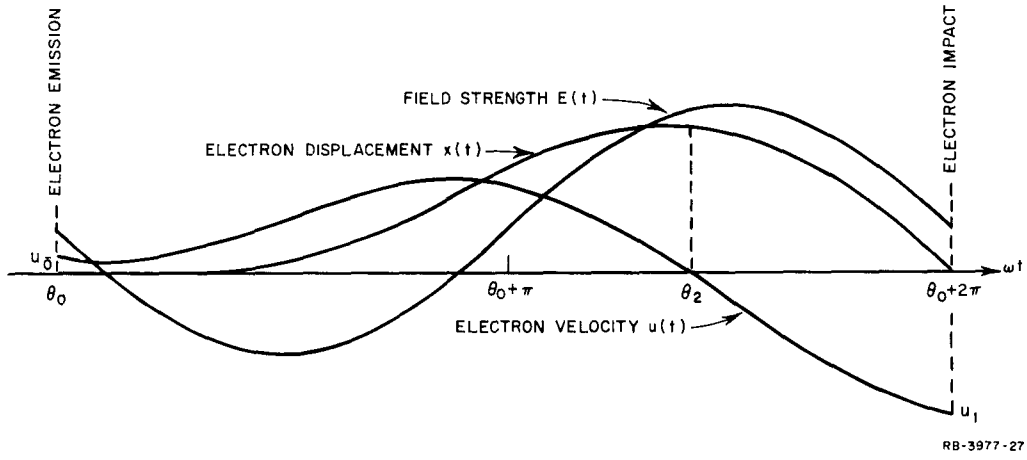

FIG. 2 ILLUSTRATION OF THE RELATIONSHIP BETWEEN ELECTRIC FIELD AND ELECTRON VELOCITY AND DISPLACEMENT IN ONE-SIDED DISCHARGE

II THEORY

A. General Analysis

In the analysis of one-sided multipacting it will be assumed that space-charge effects are negligible, so that when RF and dc voltages are applied between parallel plane electrodes as illustrated in Fig. 3, the instantaneous electric field strength in the gap is

$$E(t) = \frac{V_{dc}}{d} + \frac{V_{rf}}{d} \sin \omega t \tag{1}$$

where d is the electrode spacing and V_{dc} and V_{rf} are the applied dc and RF voltages, respectively. The acceleration of an electron will then be

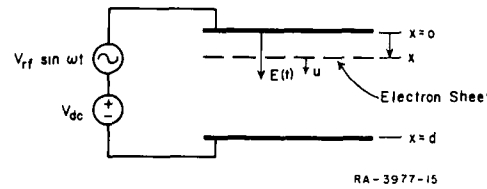

FIG. 3 DIAGRAM OF MULTIPACTOR GEOMETRY

of the form

$$\frac{d^2x}{dt^2} = - \frac{e\ V_{dc}}{md} (1 + \alpha \sin \omega t) \tag{2}$$

where e/m is the ratio of electron charge to mass and $\alpha = V_{rf}/V_{dc}$ is the ratio of the peak RF voltage to the dc voltage. Integrating Eq. (2) once to obtain the electron velocity and a second time to obtain the electron displacement yields

$$\frac{dx}{dt} = u_o + \frac{e\ V_{dc}}{\omega dm} [\theta_o - \omega t + \alpha (\cos \omega t - \cos \theta_o)] \tag{3}$$

and

$$\frac{x}{d} = \frac{u_o}{\omega d}(\omega t - \theta_o) + \frac{e V_{dc}}{\omega^2 d^2 m}\left\{-\frac{(\omega t - \theta_o)^2}{2} + \alpha\left[\sin \omega t - \sin \theta_o - (\omega t - \theta_o)\cos \theta_o\right]\right\} \tag{4}$$

where it has been assumed that the electron is emitted at $\omega t = \theta_o$ with an initial velocity u_o and zero initial displacement as indicated in Fig. 2.

For one-sided multipacting to occur, it is stipulated that the electron emitted at $\omega t = \theta_o$ must return to the electrode at the end of the RF cycle with sufficient energy to produce at least one secondary electron. Thus if u_1 (see Fig. 2) is the magnitude of the electron velocity when it has the required impact energy, we obtain from Eq. (3) the condition

$$\left.\frac{dx}{dt}\right|_{\omega t = \theta_o + 2\pi} = -u_1 \geq u_o - 2\pi \frac{e V_{dc}}{\omega d m} \quad .$$

Defining the normalized bias voltage $v_d = \frac{e/m}{\omega^2 d^2} V_{dc}$, this becomes

$$v_d \geq \frac{k + 1}{2\pi \Theta} \tag{5}$$

where $\Theta = \frac{\omega d}{u_o}$ and, following Gill and von Engel, $k = \frac{u_1}{u_o}$. When the condition that the electron must return to the emitting electrode at the end of one RF cycle (when $\omega t = \theta_o + 2\pi$) is applied to Eq. (4) we obtain

$$v_d = \frac{1}{\Theta(\pi + \alpha \cos \theta_o)} \quad . \tag{6}$$

Thus for a given frequency, gap width, and RF voltage, one-sided multipacting cannot occur unless the dc bias voltage defined by Eq. (6) exceeds the minimum value defined by Eq. (5). The range of RF voltages over which multipacting can occur can be determined from the physical limitations on the electron displacement. The maximum displacement

cannot exceed the gap width $\underline{d}$ lest the electron be lost to the opposite electrode, and the minimum displacement between emission at $\omega t = \theta_o$ and impact at $\omega t = \theta_o + 2\pi$ must be greater than zero if the electron is to escape from the electrode after it is emitted. Since these maximum and minimum displacements occur when the velocity is zero, the phase at these points can be determined by setting $\frac{dx}{dt}$ equal to zero in Eq. (3). This result, combined with Eq. (6), yields

$$\omega t - \theta_o - \pi - \alpha \cos \omega t = 0 \tag{7}$$

which can be solved for

$$\omega t = \theta_1 = \text{phase at which x is minimum}$$

and

$$\omega t = \theta_2 = \text{phase at which x is maximum} \quad .$$

Substituting θ_1 in Eq. (4) and applying the condition $x_{min} > 0$ gives

$$v_d \leq \frac{\theta_1 - \theta_o}{\Theta \frac{(\theta_1 - \theta_o)^2}{2} - \alpha \Theta[\sin \theta_1 - \sin \theta_o - (\theta_1 - \theta_o) \cos \theta_o]} \quad . \tag{8}$$

Similarly, using θ_2 and the condition $x_{max} < d$ gives

$$1 > \frac{\theta_2 - \theta_o}{\Theta} + v_d \left\{ - \frac{(\theta_2 - \theta_o)^2}{2} + \alpha \left[\sin \theta_2 - \sin \theta_o - (\theta_2 - \theta_o) \cos \theta_o\right] \right\} \quad . \tag{9}$$

Using a computer or graphical techniques such as those described in the Appendix, Θv_d can be eliminated between Eqs. (6) and (8) to obtain α as a function of θ_o for the minimum displacement. Similarly, eliminating v_d between Eqs. (6) and (9) yields α as a function of θ_o

with Θ as a parameter for the maximum displacement. Figure 4 is a plot of α as a function of θ_o, with Θ v_d as a parameter, from Eq. (6). Also shown in the figure are the limits imposed by the minimum displacement and the maximum displacement.

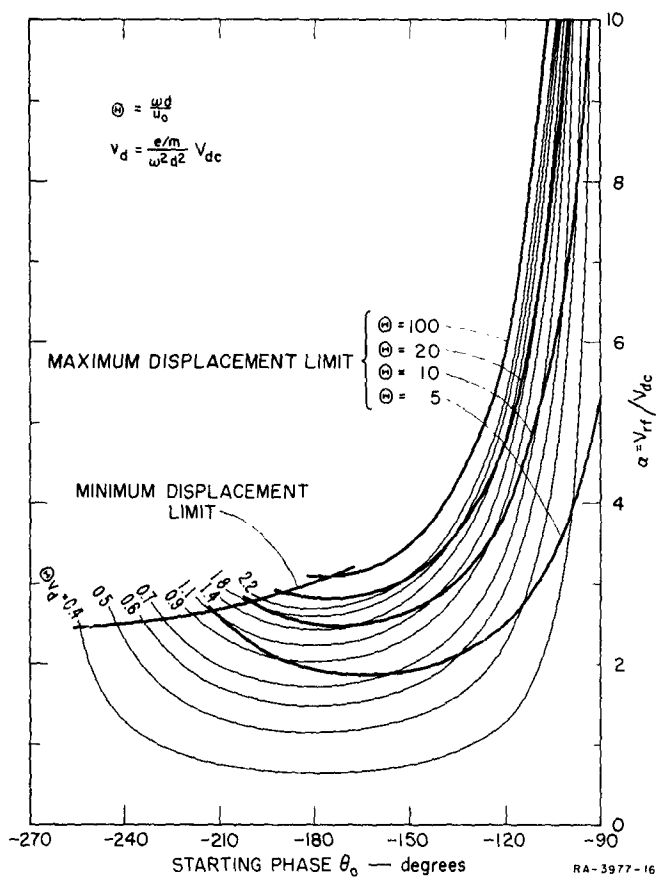

FIG. 4 PLOT OF α AS A FUNCTION OF STARTING PHASE WITH Θ v_d AS A PARAMETER

The constant- Θ v_d curves in the figure indicate the relation between the RF voltage (which is proportional to α when v_d is constant) and the

emission phase θ_o required to satisfy the condition that the electron return to the electrode at the end of the RF cycle (at $\omega t = \theta_o + 2\pi$). If the electron is emitted earlier than the phase defined by the minimum displacement limit (for the particular Θ v_d under consideration) the net field in the gap will pull the electron back to the electrode shortly after it is emitted, and the electron will be lost. If the electron is emitted after the phase defined by the minimum displacement limit, however, the electron will not be lost to the emitting electrode because the net field reverses and pulls it away from the electrode. Similarly, the maximum displacement limit shown in Fig. 4 defines the gap voltage and starting phase condition for which the maximum displacement of the electron at $\omega t = \theta_2$ (see Fig. 2) is equal to the gap width $\underline{d}$. If the computed maximum displacement were greater than the gap width, the electron would strike the opposite electrode and be lost (or, perhaps, a two-sided mode would be generated).

The analysis thus far has assumed that all secondary electrons have the same energy at emission, and that only those electrons which return to the emitting electrode precisely $2\pi/\omega$ seconds after they are emitted are of interest. Considerations of phase similar to those of Abraham[8] and Krebs,[9,10] however, indicate that even though the electrons display a distribution of emission energies and transit times, they tend to focus or "bunch" to a stable phase. To demonstrate this phase-focusing property of the discharge, let $x/d = 0$ at the phase of electron arrival, $\omega t = \theta_A$, in Eq. (4). Replacing $\theta_A - \theta_o$ by T and rearranging, we get

$$T^2 - 2\left[\frac{1}{\Theta\, v_d} - \alpha \cos\theta_o\right] T - 2\alpha \sin(T + \theta_o) + 2\alpha \sin\theta_o = 0 \quad .$$

Differentiating with respect to α and solving for $dT/d\alpha$, we obtain

$$\frac{dT}{d\alpha} = \frac{-T\cos\theta_o + \sin(T + \theta_o) - \sin\theta_o}{T - \frac{1}{\Theta\, v_d} + \alpha\left[\cos\theta_o - \cos(T + \theta_o)\right]} \quad . \tag{10}$$

Of particular interest in the phase-stability problem is the manner in which the transit time $t = \frac{T}{\omega}$ varies with the applied RF voltage (or α,

if v_d is constant) in the vicinity of the synchronous condition $T = 2\pi$. Thus letting $T = 2\pi$ in Eq. (10), we obtain

$$\frac{dT}{d\alpha} = \frac{-2\pi \cos \theta_o}{2\pi - \frac{1}{\Theta v_d}} \quad . \tag{11}$$

Now since $\Theta v_d > \frac{1}{2\pi}$ and $-90^\circ > \theta_o > -270^\circ$ [see Eq. (5) and Fig. 4], $dT/d\alpha$ is positive in the region of interest. That is, an increase in the RF voltage will increase the transit time of the electron.

To see how this result affects phase stability, a constant-Θv_d curve from Fig. 4 is redrawn in Fig. 5. For a given applied RF voltage corresponding to α_1 in Fig. 5, there are two synchronous phase values θ_{01} and θ_{02}. Consider now the case when the starting phase θ_o is slightly less (earlier) than θ_{02}. Then the applied voltage is less than that required for synchronous operation, and, by Eq. (11), the transit time is

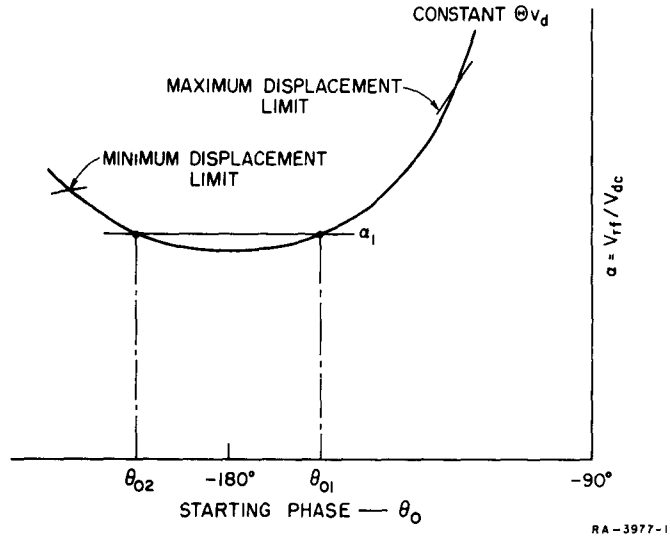

FIG. 5 ILLUSTRATION OF PHASE-STABILITY RELATIONS

somewhat less than the synchronous value of $t = 2\pi/\omega$, so that the starting phase for the next cycle is still earlier. Succeeding starting

phases thus tend to be farther and farther from the synchronous phase θ_{02}. For starting phases between θ_{01} and θ_{02}, however, the applied RF voltage is greater than that required for synchronism, so that transit times are longer than the synchronous value and the succeeding starting phases tend to move from θ_{02} toward θ_{01}. Similarly, for $\theta_o > \theta_{01}$, the applied RF voltage is lower than the synchronous value so that transit times are too short, and the succeeding starting phases approach θ_{01} from the right. Thus it is seen that θ_{01} is a stable, synchronous starting phase about which the electrons tend to bunch. θ_{02} is a synchronous phase, but an unstable one, because the starting phase tends to diverge away from θ_{02}.

It is now possible to determine the range of RF voltages over which stable one-sided multipacting can occur. For a given value of the product $\Theta\, v_d$, the preceding analysis shows that stable discharges can occur only for starting phases in the range $-180^\circ \leq \theta_o \leq -90^\circ$. Since the minima of the constant - $\Theta\, v_d$ curves occur at $\theta_o = -180^\circ$, the minimum RF voltage will correspond to the value of α at $\theta_o = -180^\circ$. Thus we can substitute $\theta_o = -180^\circ$ in Eq. (6) and, after rearranging, get

$$v_r = \pi\left(v_d - \frac{1}{\Theta\,\pi}\right) \tag{12}$$

where

$$v_r = \alpha v_d = \frac{e\,V_{rf}}{\omega^2 d^2 m} \tag{13}$$

is the normalized RF voltage. The lower RF threshold is therefore represented by a straight line of slope π in the v_d-v_r plane as indicated in Fig. 6. (For large values of Θ, such as $\Theta = 100$ in Fig. 4, the lower threshold at high bias values is determined by the minimum displacement limit rather than by $\theta_o = -180^\circ$. The lower threshold curve in this case deviates from the straight line. The deviation is very slight, however, as is illustrated in Fig. 7.)

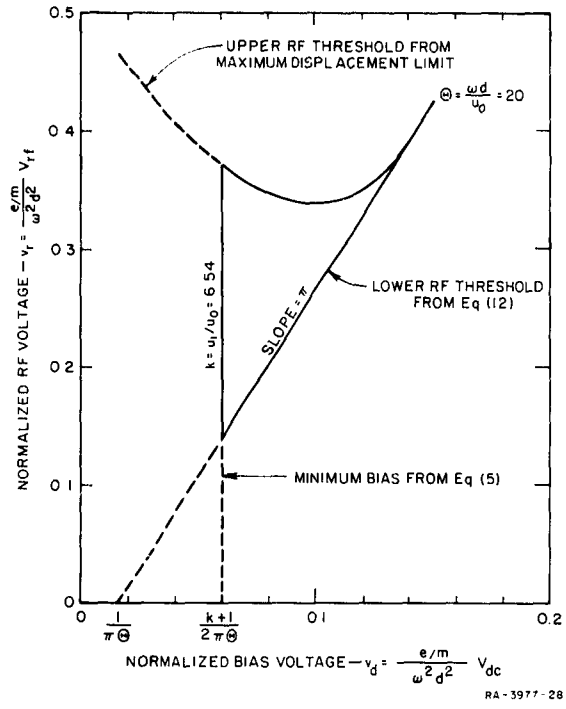

FIG. 6 ILLUSTRATION OF THE UPPER AND LOWER RF THRESHOLD AND MINIMUM BIAS FOR ONE-SIDED MULTIPACTOR DISCHARGE

The upper RF threshold voltage is determined by the maximum displacement limit imposed by Eq. (9) and shown in Fig. 4. For a given Θ, the values of α and Θ v_d along the maximum displacement curve can be read directly from Fig. 4. The normalized RF and bias voltage at each point along the upper breakdown curve can thus be obtained from

$$v_d = \frac{\Theta\, v_d}{\Theta} \quad \text{and} \quad v_r = \alpha v_d \quad .$$

An upper breakdown curve so obtained for $\Theta = 20$ is also illustrated in Fig. 6.

As can be seen, the upper and lower breakdown curves approach each other as the bias voltage is increased until a cutoff bias is reached

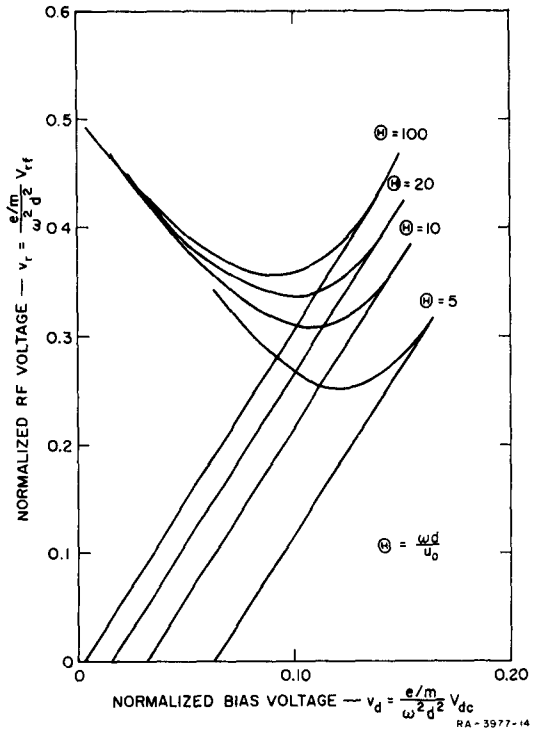

FIG. 7 UPPER AND LOWER RF THRESHOLD VOLTAGES AS FUNCTIONS OF BIAS VOLTAGE

beyond which one-sided multipacting cannot occur. When the lower limit on bias voltage, as defined by Eq. (5) and illustrated in Fig. 6, is combined with the upper and lower RF threshold curves, a closed region in the v_d-v_r plane is obtained. One-sided multipactor discharges can occur anywhere within this closed region. A family of upper and lower breakdown curves for four values of the parameter Θ are shown in Fig. 7.

It is of interest at this point to compare the region of one-sided discharge with the region of two-sided discharge predicted by Milazzo. Since Milazzo's analysis was based on the assumption of zero emission velocity and an impact velocity equal to or greater than zero, the corresponding one-sided analysis requires that $\Theta = \infty$ and that the minimum

bias be determined from Eq. (5) with $u_o = 0$. The normalized minimum bias voltage is thus

$$v_d = \frac{u_1}{2\pi\ \omega\ d} \quad .$$

The assumption that the impact velocity must be equal to or greater than zero has not been made in determining the one-sided curves, since such an assumption would make the minimum bias zero and the entire lower breakdown curve would be determined by the one-sided mode. Instead, it has been assumed that a definite impact velocity u_1 is necessary for the one-sided mode to operate, so that at low bias voltages the lower breakdown voltage is determined by the two-sided mode, while at bias voltages greater than $u_1/2\pi\ \omega\ d$ the lower breakdown voltage is determined by the one-sided mode. It has also been assumed that the two-sided mode can initiate with an unstable starting phase, since experimental results appear to support this assumption. The composite breakdown region including both one-sided and two-sided modes under these conditions is indicated by the solid curve in Fig. 8.

Perhaps the most interesting feature of Fig. 8 is that it confirms the postulate that the one-sided multipactor discharge could be responsible for the minimum in the lower breakdown curve of Fig. 1. Also of interest is the fact that the one-sided mode is stable throughout the RF range for bias voltages above the minimum, whereas the two-sided mode is stable for only a very narrow range of RF voltages.

B. Higher-Order Modes

In the analysis leading to Eqs. (5) through (9) it has been required that the electron emitted at θ_o return at $\theta_o + 2\pi$. From a purely analytical standpoint, there is no reason why the electron could not return at $\theta_o + 2n\pi$, where n is an integer. If this were allowed, Eqs. (5) and (6) would become

$$v_d \geq \frac{1 + k}{2n\pi\ \Theta} \qquad (5')$$

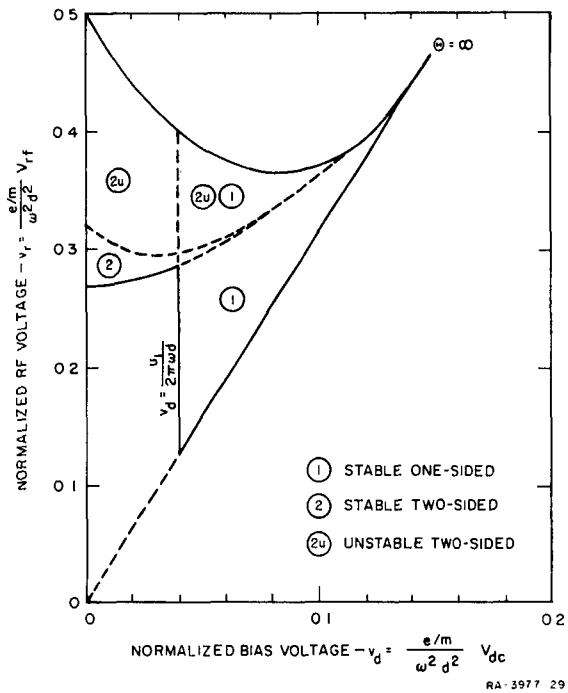

FIG. 8 BIASED MUL . 'PACTOR DISCHARGE REGION INCLUDING ONE-SIDED AND TWO-SIDED MODES

and

$$v_d = \frac{1}{\Theta\,(n\pi + \alpha \cos\theta_o)} \quad . \tag{6'}$$

The lower breakdown curve is obtained by letting $\theta_o = -180^\circ$ in Eq. (6'), and Eq. (5') defines the minimum bias for the higher-order modes. The lower breakdown curves for the higher-order modes can thus be plotted as in Fig. 9. Although the solution for the upper breakdown curve is much more difficult and has not been carried out, examination of the effects of the higher-order modes on Eqs. (7) and (9) suggests that as the bias approaches zero, the breakdown voltage v_r approaches 0.5 as it does in the fundamental mode.

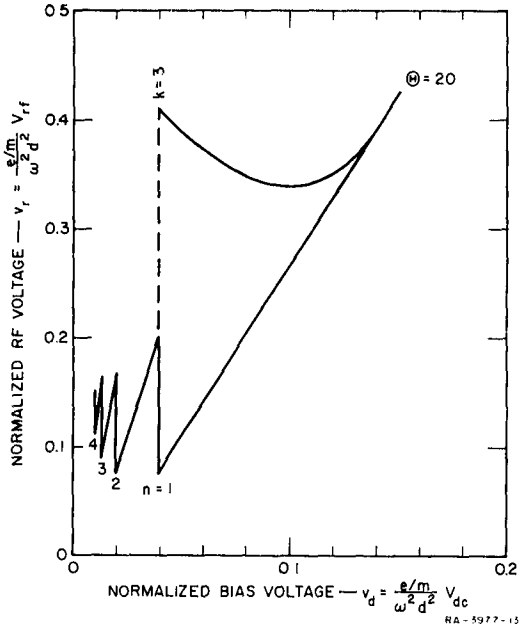

FIG. 9 LOWER RF THRESHOLD VOLTAGE FOR HIGHER-ORDER MODES

The minimum bias and lower breakdown curves as shown in Fig. 9, however, indicate that the presence of higher-order modes would eliminate, or at least lower, the minimum bias cutoff that has been observed in multipactor experiments. Consideration of emission energies and the impact energy required to produce a secondary emission coefficient greater than unity also casts doubt on the possibility of the higher-order modes existing. Since the electron is away from the electrode for an even number of half-cycles, it can gain no net energy from the RF field. Thus the dc field supplies all of the energy that the electron gains, while the RF field merely serves to suspend the electron in space while it absorbs energy from the dc field. The RF field cannot prevent the electron from returning to the electrode for more than one cycle, however, unless the dc field is so weak that the electron absorbs less energy from the field than it gives up to the field during one cycle. If it is assumed that the electron absorbs slightly less than

its emission energy in one cycle, so that after two cycles its net energy is almost three times its emission energy, it might have sufficient energy to produce one secondary electron. The n = 2 mode would thus be possible for a material having high emission energy and requiring low impact energy for unity secondary coefficient. It is hardly conceivable, however, that modes higher than the second could operate with any of the cathode materials presently known.

C. Limitations of the Theory

In deriving the theoretical curves of Fig. 7, several idealizations were made to make the analysis more tractable. While none of these idealizations is of sufficient importance to drastically alter the results, some of them may contribute to noticeable deviations from the values predicted in the figure. In the analysis, for example, it has been assumed that the electrons travel in a sheet of infinitesimal thickness, whereas in reality, because of the variations in emission velocity, the electrons travel in a cloud of finite thickness. Since the displacement $\underline{x}$ in Eq. (4) is approximately the position of the center of this cloud, when the maximum displacement $x = d$ is attained, approximately half of the electrons in the cloud are lost to this passive electrode. The RF voltage would thus have to be reduced somewhat below the predicted value to reduce the rate of loss at the passive electrode to approximately the rate of production at the active electrode.

It is also possible that, because of the distribution of secondary emission energies, the value of Θ varies somewhat along the contour of threshold voltages. For certain RF and bias voltages, the phase may focus toward a value corresponding to an emission energy slightly greater than the most probable energy, while for other voltages, the phase might focus toward a value corresponding to an emission energy slightly less than the most probable value. It might be expected, for instance, that the effective emission energy for the lower breakdown curve would be slightly higher than that for the upper curve, since for the lower curve the electrons are emitted against a retarding field, and some of the low-energy electrons are forced back to the electrode. The average energy

of the escaping electrons would certainly be larger for conditions pertaining to the lower breakdown curve. This higher average energy could result in a higher effective emission energy and a lower value of Θ.

Variations in Θ may also result from an oxide film on the active electrode. Experience with multipacting in two-sided modes suggests that even electrodes that appear to be clean and outgassed may actually have a thin film of oxide on the surface. Experiments with the biased two-sided multipactor discharge have illustrated the effects of these films in an interesting manner. Since the oxides are often insulating or only partially conducting, charge can accumulate on the oxide surface and develop very high dc field strengths in the film. When the dielectric strength of the film is exceeded, the film breaks down and a visible flash or scintillation is observed. These scintillations, which are believed to be the same as those described by others in connection with the Malter effect,[11] have been observed on the negative electrode when brass or aluminum electrodes were used. With copper electrodes, however, the scintillations are observed on the positive electrode. It is postulated that the peculiar behavior of copper in this respect results from the fact that the copper-cuprous oxide junction offers little resistance to the flow of electrons from the copper to the oxide, but it impedes the flow of electrons from the oxide to the copper. Electrons or negative ions can thus accumulate on the oxide film and distort the field at the electrode surface of copper electrodes in much the same manner as positive ions are purported to accumulate on the oxides of aluminum and other materials displaying the Malter effect. Such a charged film can affect the coefficient of secondary emission and the effective emission energy as well as partially nullify the dc bias voltage. Since the film is bombarded by the electron cloud each cycle, these effects may also be frequency-dependent.

There is also some uncertainty as to the interpretation of the results of the analysis for bias voltages near the maximum bias cutoff. In the stability analysis it was argued that only starting phases between -180° and -90° could be considered stable. The phase of electrons

emitted earlier than -180° would tend toward the stable phase in succeeding cycles, however, if the initial phase were between the two synchronous phase points (see Fig. 5). Note in Fig. 4, now, that for values of Θ less than about 20, the upper limit on α, for the larger Θ v_d values, is determined by the minimum displacement limit rather than the maximum displacement limit, if the unstable starting phases are allowed. Abraham's work with the two-sided modes in microwave cavities strongly suggests that breakdown under conditions of decreasing RF voltage can initiate under unstable phase conditions, and can load the RF circuit sufficiently to reduce the voltage to a stable phase region.[8] It is suspected that this phenomenon also occurs in the one-sided mode, so that the minimum displacement, rather than the maximum displacement, determines the upper breakdown voltage at the higher bias value. If such were the case, the upper RF breakdown voltage at the higher bias voltages would be, relatively, higher than that at lower bias voltages. As will be seen below, the experimental data suggest that the result of unstable initiation may be an increase in the breakdown voltage of sufficient magnitude to cancel the reduction caused by electron cloud thickness.

III EXPERIMENTAL VERIFICATION

Since the foregoing analysis indicated the possibility of the one-sided mode, which, for certain conditions, could occur at lower RF voltages than the two-sided mode (see Fig. 8), an experiment was designed in which the existence of the one-sided mode could be verified. The apparatus for the experiment is shown schematically in Fig. 10. The electrodes, which were discs 15 centimeters in diameter, formed part of the capacitance of a tuned tank circuit. The tank coil was constructed

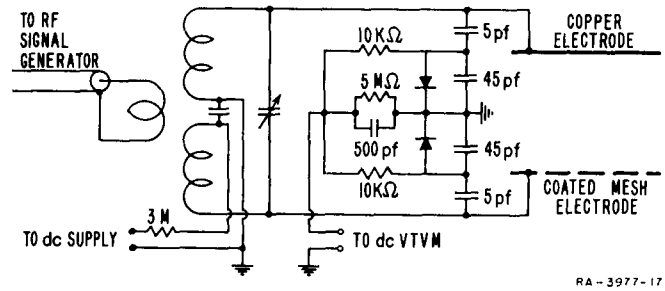

FIG. 10 SCHEMATIC DIAGRAM OF EXPERIMENTAL APPARATUS

of two coils connected in series through a low-impedance capacitance, across which the dc bias was applied. Because under certain discharge conditions the one-sided mode was found to be difficult to detect visually or by its loading on the RF circuit, the bias was applied through a high resistance so that when breakdown occurred and the gap became conducting, a voltage drop appeared across the series resistance. Also shown in the figure is the balanced rectifier used to detect the RF voltage across the plates. Commercial copper which had been abrasively cleaned was used for the multipactor electrode. The opposite electrode was fabricated from a wire mesh and coated with lamp black to reduce secondary emission, thereby preventing the two-sided mode. The entire electrode structure, which is shown in Fig. 11, was placed in a 15-inch

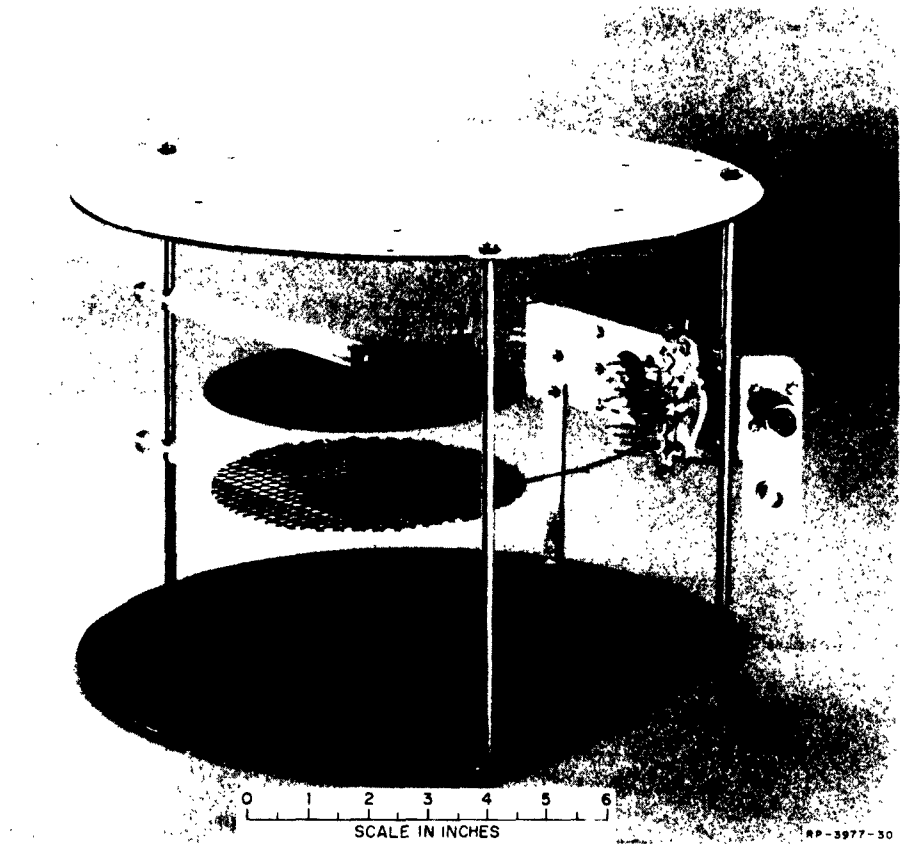

FIG. 11 EXPERIMENTAL APPARATUS FOR DETERMINING THE REGION OF ONE-SIDED MULTIPACTOR DISCHARGE

bell jar equipped with an oil diffusion pump. As a check on the effectiveness of the wire mesh and lamp black in preventing the two-sided mode, the RF voltage was increased slowly, without dc bias, through the range in which two-sided multipacting normally occurs. This procedure was repeated using moderate bias voltages with the coated mesh positive. No discharges were observed in either case.

The one-sided multipactor experiment was conducted at 34.9 and 54.5 megacycles per second with a gap width of 5.4 centimeters at a pressure of about 0.1 micron. The measured values of upper and lower RF threshold

voltages and minimum dc bias are shown in normalized form in Fig. 12. The threshold voltages were determined by setting one of the voltages (dc, for example) and changing the other (RF) until breakdown was

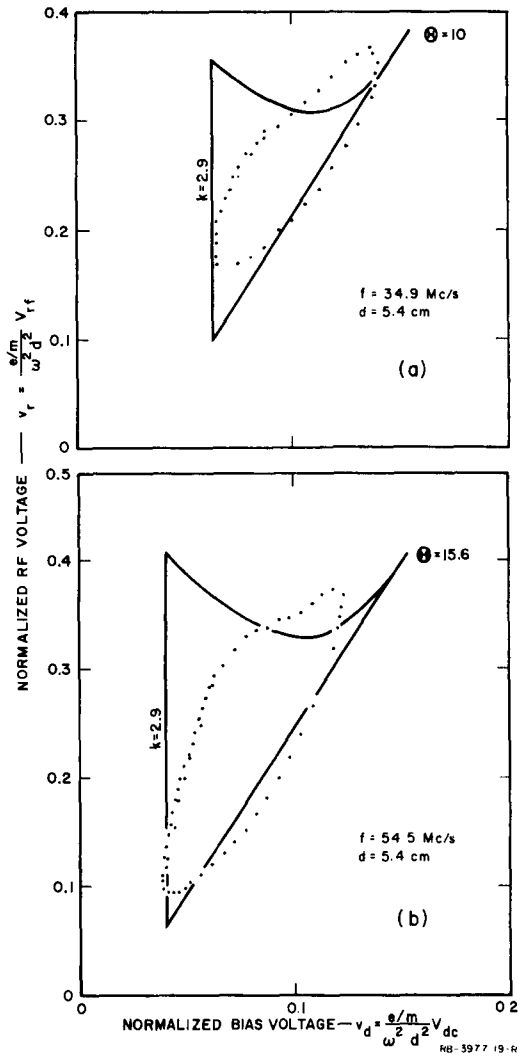

FIG. 12 EXPERIMENTAL THRESHOLD CONTOUR WITH CLOSEST-FITTING THEORETICAL CONTOUR SUPERIMPOSED

indicated by a drop in the RF voltage, or in the case of weak discharges, by a drop in the dc voltage across the gap. Thus all of the data points represent conditions for which the discharge initiates, rather than conditions at which an established discharge is extinguished.

Also shown in Fig. 12 are the closest fitting theoretical breakdown curves. Considering the idealizations of the theory in which the finite thickness of the electron cloud, the effect of oxide films and other contaminants, the distribution of emission energy, and the possibility of discharges initiating in an unstable region have been disregarded, it is felt that the experimental data are in good agreement with the predicted values. The values of Θ for the theoretical curves shown in the figure were chosen to be of the same ratio, 1.56, as the RF frequencies, since the gap width $\underline{d}$ was the same for both frequencies and the emission velocity u_o was assumed to be independent of frequency. Using these values of Θ in Eq. (5), $\underline{k}$ was found to be approximately 2.9. This value of $\underline{k}$ is in excellent agreement with the value 3.0 assumed by Hatch and Williams for two-sided multipacting.

The experimental data are perhaps more useful when they are plotted as true voltages rather than in the normalized form. The RF breakdown voltage is therefore plotted as a function of the dc bias voltage for the two experimental frequencies in Fig. 13. As the figure illustrates, the size of the region over which the one-sided mode operates is quite frequency-dependent. In addition to the experiments performed at 34.9 and 54.5 megacycles, the experiment was attempted at a frequency of 28.6 megacycles. Using the 5.4 centimeter gap, however, it was not possible to initiate the discharge at the lower frequency, implying that the minimum bias required by Eq. (5) exceeded the cutoff bias.

One-sided multipactor experiments were also conducted at 35 megacycles using yellow brass and cold rolled steel for the multipacting electrode. The results in both cases were very similar to those obtained with copper at 34.9 megacycles.

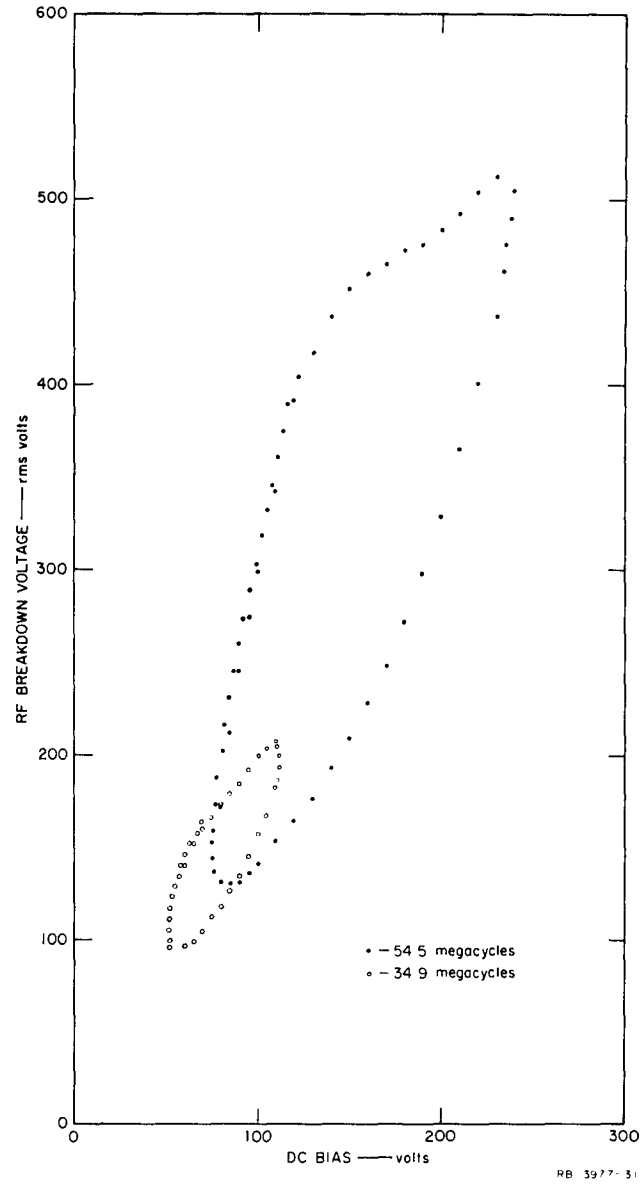

FIG. 13 EXPERIMENTAL DATA OF FIG. 12 PLOTTED IN TRUE RF AND BIAS VOLTAGES

IV CONCLUDING REMARKS

The analysis and experimental program described above indicate that a one-sided mode of biased multipactor discharge does indeed exist. Unlike the two-sided discharge, which absorbs energy from the RF field, the one-sided mode absorbs energy only from the dc field. (This is true during build-up when space charge effects may be neglected; it may not be true after the discharge has developed.) The one-sided discharge thus appears as a reactive load on the RF circuit.

The practical importance of the one-sided discharge is two-fold. First, because the lower RF threshold for the one-sided mode is generally lower than the lower threshold for the two-sided modes for a given bias, the one-sided mode has the effect of lowering the threshold of RF breakdown. This effect has been demonstrated in Fig. 8 where the theoretical breakdown curves for the one-sided and two-sided modes are compared, and in Fig. 1 where the experimental data show the reduction in RF threshold voltage as the bias is increased. Because of this property of the discharge, the use of dc bias to prevent multipactor discharges requires careful consideration, since insufficient bias, or partial failure of the bias system, can result in a lower RF breakdown voltage than would obtain in the absence of bias.

The second property of the one-sided discharge that is of practical concern is its effect on circuit elements. Because the one-sided discharge is predominately reactive, it can be presumed that the one-sided discharge *per se* does not absorb appreciable power from the RF system. The reactive loading associated with the discharge can detune resonant RF circuits, however, thereby seriously degrading the performance of the RF system. In addition, it has been observed in experiments with biased multipactor discharges that a discharge often initiates in the one-sided mode, and with a slight increase in RF voltage, makes a transition to the two-sided mode. The presence of the one-sided discharge thus appears to lower the threshold of the power-consuming two-sided mode.

In view of these properties of the one-sided mode and the properties of the other modes, there is little doubt that multipactor discharges will pose a problem in many RF components on spacecraft or satellites. Reports of satellite RF equipment malfunctions which appear to be related to multipactor discharges have, in fact, already been reported to the authors by other contractors connected with the space program. It seems fitting, therefore, that the practical implications of the multipactor discharge be more thoroughly investigated to determine the limitations this breakdown mechanism places on specific components such as antennas and associated equipment, and to determine the effect of ambient ionization of the degree found in the ionosphere on RF breakdown voltages. Such investigations are currently being implemented under the continuing multipactor study program.

APPENDIX

GRAPHICAL SOLUTION FOR ELECTRON DISPLACEMENT LIMITS

APPENDIX

GRAPHICAL SOLUTION FOR ELECTRON DISPLACEMENT LIMITS

To obtain a graphical solution of Eqs. (6), (8), and (9) for the displacement limits of Fig. 4, it is first necessary to solve for the roots θ_1 and θ_2 of Eq. (7). To obtain these roots graphically, Eq. (7) can be rewritten in the form

$$\frac{1}{\alpha}\left[\omega t - (\theta_o + \pi)\right] = \cos \omega t \quad . \tag{A-1}$$

The left side of Eq. (A-1) is a linear function of ωt with slope $1/\alpha$ and an intercept at $\omega t = \theta_o + \pi$. The right side is the pure cosine function, independent of α and θ_o. The solutions of Eq. (A-1) can be readily obtained by plotting a cosine curve and, on the same coordinates, plotting a straight line of slope $1/\alpha$ passing through zero at $\theta_o + \pi$ as shown in Fig. A-1. The intersection of the line with the cosine curve

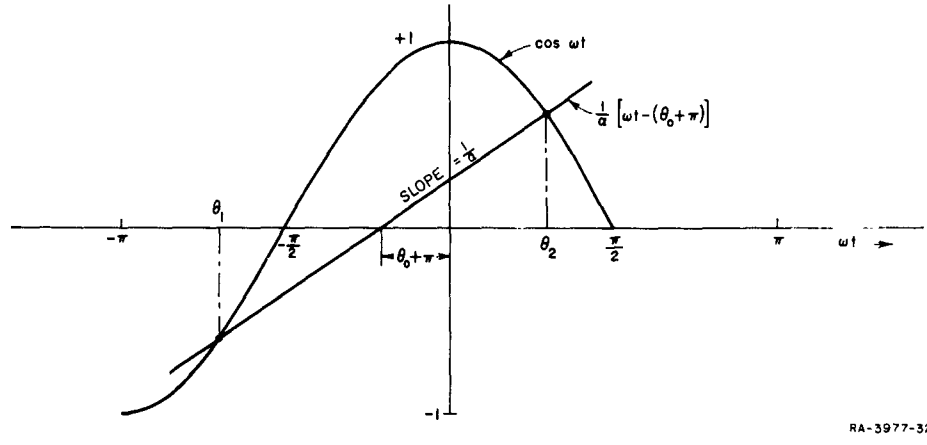

FIG. A-1 ILLUSTRATION OF GRAPHICAL SOLUTION FOR θ_1 AND θ_2

to the left of the origin defines θ_1, while the intersection to the right of the origin defines θ_2. Failure to obtain an intersection to

the left of the origin may be interpreted as meaning that the electron emitted against the dc field is not decelerated sufficiently to reverse its direction of travel before the net field reverses and accelerates it away from the electrode. In such cases θ_1 does not exist, and the minimum displacement limit does not apply.

For each set (α, θ_o), the solution provides two sets (α, θ_o, θ_1) and (α, θ_o, θ_2) which can be used in Eqs. (8) and (9), respectively, to compute values of $\Theta\ v_d$ [the inequalities of Eqs. (8) and (9) are replaced by equalities to define the minimum and maximum displacement limits]. In addition, from Eq. (6) we can compute $\Theta\ v_d$ as a function of α and θ_o. We thus have three sets of $\Theta\ v_d$ (α, θ_o) as follows:

$$\Theta\ v_d = \frac{1}{\pi + \alpha \cos \theta_o} \tag{A-2}$$

from Eq. (6) which, defines the condition that the electron return to the emitting electrode at $\omega t = \theta_o + 2\pi$;

$$\Theta\ v_d = \frac{\theta_1 - \theta_o}{\frac{(\theta_1 - \theta_o)^2}{2} - \alpha \left[\sin \theta_1 - \sin \theta_o - (\theta_1 - \theta_o) \cos \theta_o\right]} \tag{A-3}$$

from Eq. (8), which defines the condition that the electron's minimum displacement, between the time of its emission at $\omega t = \theta_o$ and the time of its return to the electrode at $\omega t = \theta_o + 2\pi$, be zero; and

$$\Theta\ v_d = \frac{\Theta - (\theta_2 - \theta_o)}{-\frac{(\theta_2 - \theta_o)^2}{2} + \alpha \left[\sin \theta_2 - \sin \theta_o - (\theta_2 - \theta_o) \cos \theta_o\right]} \tag{A-4}$$

from Eq. (9), which defines the condition that the electron's maximum displacement between $\omega t = \theta_o$ and $\omega t = \theta_o + 2\pi$ be $\underline{d}$.

It is desired to obtain α as a function of θ_o with $\Theta\ v_d$ as a parameter (as in Fig. 4) along the maximum displacement limit and α as a function of θ_o along the minimum displacement limit. Since $\Theta\ v_d$ is

the dependent variable, this is most easily achieved by plotting $\Theta\ v_d$ as a function of θ_o with α as a parameter from Eq. (A-2), and on the same coordinates, plotting $\Theta\ v_d$ from Eqs. (A-3) and (A-4). The intersections of the constant-α curves from Eqs. (A-2) and (A-3) are points on the minimum displacement limit, and the intersections of the constant-α curves from Eqs. (A-2) and (A-4) are (for a given Θ) points on the maximum displacement limit.

Figure A-2 illustrates the method for the constant-α curves of Eqs. (A-2) and (A-4) when $\Theta = 10$. For a given α, the intersection of the constant-α curves defines the value of the starting phase θ_o for which an electron that returns to the emitting electrode at $\omega t = \theta_o + 2\pi$ has a maximum displacement $x = d$. The desired curve $\alpha\ (\theta_o)$ for the maximum displacement limit can thus be plotted from these values of α and θ_o. The procedure can be repeated for other values of Θ to obtain the remaining maximum displacement limits of Fig. 4.

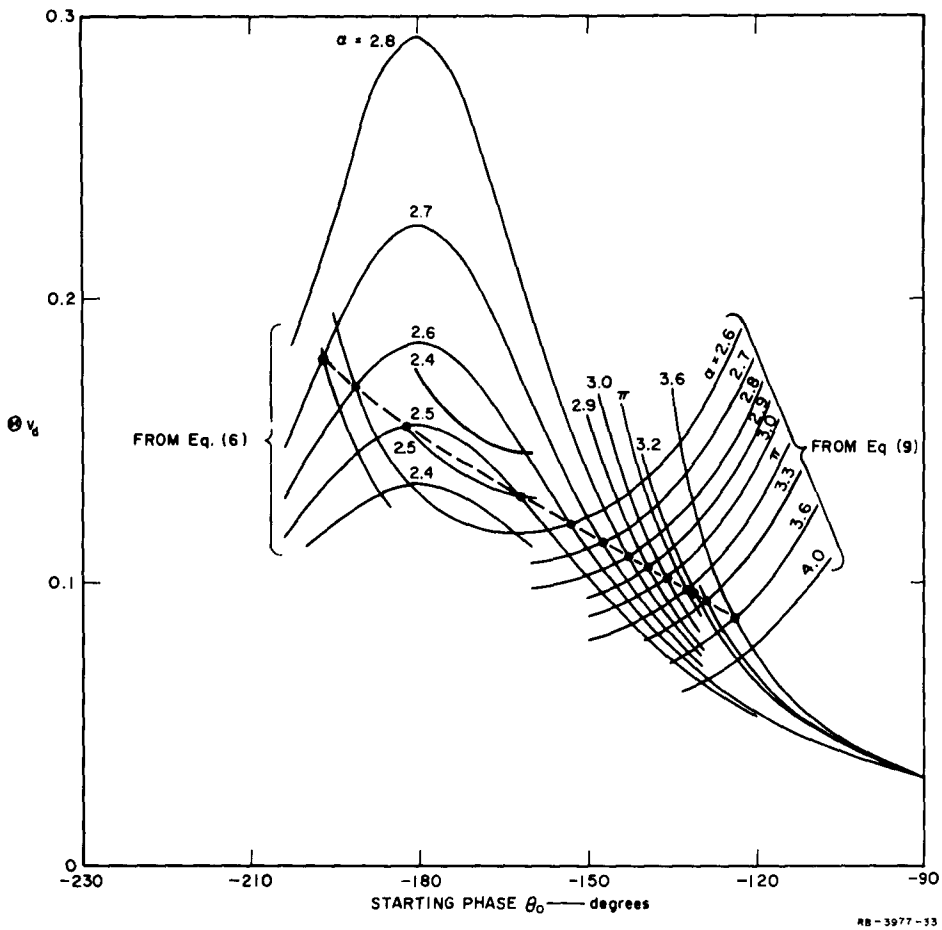

FIG. A-2 ILLUSTRATION OF THE GRAPHICAL SOLUTION OF EQS. (6) AND (9) TO OBTAIN THE MAXIMUM DISPLACEMENT LIMIT

REFERENCES

1. E. W. B. Gill and A. von Engel, "Starting Potentials of High-Frequency Gas Discharges at Low Pressure," Proc. Roy. Soc. (London) 192A, pp. 446-63 (1948).

2. G. Francis and A. von Engel, "The Growth of the High-Frequency Electrodeless Discharge," Trans. Roy. Soc. (London) 246A, pp. 143-80 (1953).

3. A. J. Hatch and H. B. Williams, "The Secondary Electron Resonance Mechanism of Low-Pressure High-Frequency Gas Breakdown," J. Appl. Phys. 25, 4, pp. 417-23 (1954).

4. A. J. Hatch and H. B. Williams, "Multipacting Modes of High-Frequency Gaseous Breakdown," Phys. Rev. 112, 3, pp. 681-85 (1958).

5. K. Bol, "The Multipactor Effect in Klystrons," IRE National Convention Record, Vol. 2, Pt. 3, pp. 151-55 (1954).

6. C. Milazzo, "Study of Multipactor Discharge in the Presence of a dc Bias," Tech. Memo TM 61-15, General Electric Co., Palo Alto, California (13 March 1961).

7. S. C. Brown, Basic Data of Plasma Physics, pp. 214-17 (John Wiley and Sons, Inc., New York, New York, 1959).

8. W. G. Abraham, "Interactions of Electrons and Fields in Cavity Resonators," Ph.D. Dissertation, Stanford University, Stanford, California (1950).

9. K. Krebs, "Uber die Pendelvervielfachung von Sekundärelektronen in Hochfrequenten Feldern," Z. angew. Phys. Bd 2, H 10, 400-11 (1950).

10. K. Krebs and H. Meerbach, "Die Pendelvervielfachung von Sekundärelektronen," Ann. Physik 15, pp. 189-206 (1955).

11. K. G. McKay, "Secondary Electron Emission," Advances in Electronics, Vol. I, 117-120, Academic Press, Inc., New York (1948).

TECHNICAL REPORTS IN THIS SERIES

Reports Issued on Contract AF 19(122)-78

1. "Electric Dipoles in the Presence of Elliptic and Circular Cylinders," by W. S. Lucke, September 1949.

2. "Asymmetrically Fed Antennas," by C. T. Tai, November 1949.

3. "Double Fed and Coupled Antennas," by C. T. Tai, February 1949.

4. "Equivalent Radii of Thin Cylindrical Antennas with Arbitrary Cross Sections," by Carson Flammer, March 1950.

5. "Use of Complementary Slots in Aircraft Antenna Impedance Measurements," by J. T. Bolljahn, February 1950.

6. "Wing-Cap and Tail-Cap Aircraft Antennas," by J. V. N. Granger, March 1950.

7. "Investigation of Current Distribution on Asymmetrically-Fed Antennas by Means of Complementary Slots," by R. M. Hatch, Jr., February 1950.

8. "Electromagnetic Resonance Phenomena in Aircraft Structures," by A. S. Dunbar, May 1950.

9. "The Effect of a Grounded Slab on the Radiation from a Line Source," by C. T. Tai, June 1950.

10. "A Method for the Calculation of Progressive-Phase Antennas for Shaped Beams," by A. S. Dunbar, June 1950.

11. "Admittance of an Open-Ended Coaxial Line in an Infinite Grounded Plane," by W. S. Lucke, June 1950.

12. "A Variational Solution to the Problem of Cylindrical Antennas," by C. T. Tai, August 1950.

13. "Uniform Progressive-Phase Antennas Having Asymmetrical Amplitude Distributions," by A. S. Dunbar, September 1950.

14. "Small Dipole-Type Antennas," by J. T. Bolljahn, September 1950.

15. "Tables of Modified Cosine Integrals," January 1951.

16. "Prolate Spheroidal Wave Functions," by Carson Flammer, February 1951.

TECHNICAL REPORTS IN THIS SERIES

Reports Issued on Contract AF 19(122)-78

1. "Electric Dipoles in the Presence of Elliptic and Circular Cylinders," by W. S. Lucke, September 1949.

2. "Asymmetrically Fed Antennas," by C. T. Tai, November 1949.

3. "Double Fed and Coupled Antennas," by C. T. Tai, February 1949.

4. "Equivalent Radii of Thin Cylindrical Antennas with Arbitrary Cross Sections," by Carson Flammer, March 1950.

5. "Use of Complementary Slots in Aircraft Antenna Impedance Measurements," by J. T. Bolljahn, February 1950.

6. "Wing-Cap and Tail-Cap Aircraft Antennas," by J. V. N. Granger, March 1950.

7. "Investigation of Current Distribution on Asymmetrically-Fed Antennas by Means of Complementary Slots," by R. M. Hatch, Jr., February 1950.

8. "Electromagnetic Resonance Phenomena in Aircraft Structures," by A. S. Dunbar, May 1950.

9. "The Effect of a Grounded Slab on the Radiation from a Line Source," by C. T. Tai, June 1950.

10. "A Method for the Calculation of Progressive-Phase Antennas for Shaped Beams," by A. S. Dunbar, June 1950.

11. "Admittance of an Open-Ended Coaxial Line in an Infinite Grounded Plane," by W. S. Lucke, June 1950.

12. "A Variational Solution to the Problem of Cylindrical Antennas," by C. T. Tai, August 1950.

13. "Uniform Progressive-Phase Antennas Having Asymmetrical Amplitude Distributions," by A. S. Dunbar, September 1950.

14. "Small Dipole-Type Antennas," by J. T. Bolljahn, September 1950.

15. "Tables of Modified Cosine Integrals," January 1951.

16. "Prolate Spheroidal Wave Functions," by Carson Flammer, February 1951.

17. "An Antenna Evaluation Method," by W. S. Lucke, April 1951.

18. "Radar Response from Thin Wires," by C. T. Tai, March 1951.

19. "The Measurement of Low-Frequency Aircraft Antenna Properties Using Electrostatic Methods," by J. T. Bolljahn, September 1951.

20. (Dropped).

21. "A Method for the Calculation of Progressive-Phase Antennas for Shaped Beams," Part II, by A. S. Dunbar, May 1951.

22. "The Prolate Spheroidal Monopole Antenna," by Carson Flammer, August 1957, issued on Contract AF 19(604)-1296.

23. "Variational Solution for the Problem of the Asymmetric Dipole," by I. Reese, August 1951.

24. "Quasi-Static Solution for Diffraction of a Plane Electromagnetic Wave by a Small Oblate Spheroid," by C. T. Tai, September 1952 [Issued on Contract AF 19(604)-266].

25. "Transmission Through a Rectangular Aperture in an Infinite Screen," by W. S. Lucke, September 1951.

Reports Issued on Contract AF 19(604)-266

26. "Improvements in Instrumentation for the Investigation of Aircraft Antenna Radiation Patterns by Means of Scale Models," by R. M. Hatch, Jr., August 1952.

27. "The Vector Wave Solution of the Diffraction of Electromagnetic Waves by Circular Disks and Apertures," by Carson Flammer, September 1952.

28. "An Investigation of the Distribution of Current on Collinear Parasitic Antenna Elements," by R. M. Hatch, Jr., August 1952.

29. "On the Theory of Diffraction of Electromagnetic Waves by a Sphere," by C. T. Tai, October 1952.

30. "High-Frequency Airborne Direction Finding," by P. S. Carter, Jr., December 1952.

31. "An Electrolytic Tank Method for Low-Frequency Loop Antennas Studies," by R. F. Reese, July 1953.

32. "Radiation from a Uniform Circular Loop Antenna in the Presence of a Sphere," by C. T. Tai, December 1952.

33. "A Computer for Use with Antenna Model Ranges," by C. E. Fisher, February 1953.

34. "Tail-Cap Antenna Radiation Pattern Studies," by J. H. Bryan, January 1953.

35. "U-H-F Tail-Cap Antenna Pattern Characteristics and Their Control," by A. R. Ellis, March 1955 [issued on Contract AF 19(604)-1296].

36. "Mutual Admittance of Slots in Cylinders," by W. S. Lucke, February 1953.

37. "Radio Interference from Corona Discharges," by R. L. Tanner, April 1953.

38. "Effects of Airframe Configuration on Low-Frequency Antenna Characteristics," by C. M. Hoblitzell, April 1953.

39. "The Effects of Thin Resistive Coatings on Low-Frequency Aircraft Antenna Performance," by C. W. Steele [issued on Contract AF 19(604)-1296] January 1956.

40. "Analysis of the Overstation Behavior of Airborne ADF Systems," by H. H. Ward, June 1954.

41. "Some Electromagnetic Problems Involving a Sphere," by C. T. Tai, April 1953.

42. "Radiation Pattern Measurements of Stub and Slot Antennas on Spheres and Cylinders," by J. Bain, April 1953.

43. "Current Distribution on Wing-Cap and Tail-Cap Antennas," by Irene C. Carswell, May 1954.

44. "A Study of Radiating Structures for Perpendicularly-Polarized Flush Radar Antennas," by Edward M. T. Jones and Seymour B. Cohn, July 1953.

45. "Radiation from Current Elements and Apertures in the Presence of a Perfectly Conducting Half-Plane Sheet," by C. T. Tai, July 1954.

46. "A Glossary of Dyadic Green's Functions," by C. T. Tai, July 1954.

47. "Horizontally Polarized Long-Slot Array," by R. C. Honey, August 1954.

Reports Issued on Contract AF 19(604)-1296

48. "Microwave Radiation from Large Finite Bodies," by Seymour B. Cohn and Tetsu Morita, January 1955.

49. "Radiation from Electric and Magnetic Dipoles in the Presence of a Conducting Circular Disk," by Carson Flammer, February 1955.

50. "A Study of Some Inherent Errors in the Three-Dimensional Raydist System," by Irene Carswell, March 1955.

51. "Operating Characteristics of Flush-Mounted Bombing Antennas," by E. M. T. Jones, November 1955.

52. "Properties of the Asymmetric Dipole," by Irene Carswell, December 1955.

53. "Notch Coupling to the Electromagnetic Resonance of a Delta-Wing Aircraft," by William L. Jones, December 1955.

54. "A Flush-Mounted Horizontally Polarized Directional Antenna," by R. C. Honey, January 1956.

55. "Radiation from a Flush-Mounted Scanning Antenna on the Nose Section of a Supersonic Aircraft," by J. K. Shimizu and T. Morita, December 1955.

56. "An Economical Logarithmic Recording System," by Lloyd A. Robinson, June 1956.

57. "Variational Formulae for Domain Functionals in Electromagnetic Theory," by Carson Flammer, March 1957.

58. "Systems Considerations for High Speed Missile Seeker Antennas," by Donald L. Margerum and E. Thomas Brandon, May 1957. Confidential.

59. "High-Strength Dielectric Materials for Very Fast Aircraft," by Henry J. Sang, March 1957.

60. "Impedance Matching Limitations with Application to the Broadband Antenna Problem," by Arthur Vassiliadis, January 1957.

61. "Shunt-Fed and Notch-Fed Aircraft Antennas," by Robert L. Tanner, July 1957.

62. "A Study of Precipitation-Static Noise Generation in Aircraft Canopy Antennas," by Joseph E. Nanevicz, September 1957.

63. "Electromagnetic Wave Propagation in a Medium with Variable Dielectric Constant $1 + kr^{-1}$," by Carson Flammer, January 1958.

Reports Issued on Contract AF 19(604)-3458

64. "The Back-Scattering Cross Sections of Missile Trails," by Carson Flammer, June 1958.

65. "Ray-Tracing and Diffraction in a Medium with Variable Permittivity and Attenuation," by James A. Cochran, October 1958.

66. "Feasibility Study of Aircraft Antennas for Forward-Scatter and Meteor-Burst Communication," by J. F. Cline, July 1959.

67. "A Study of Possibilities for Improving Space Utilization and Performance of Rhombic Antennas," by Angel Martin-Caloto, July 1959.

68. "Aerodynamic Characteristics of Trailing-Wire Antennas at Supersonic Speeds," by F. B. Harris, Jr., March 1960.

69. "Voltage Breakdown of Antennas at High Altitudes," by W. E. Scharfman and T. Morita, April 1960.

70. "A Study of Corona Discharge Noise in Aircraft Antennas," by A. Vassiliadis, August 1960.

71. "Theoretical Limitations on the Broadbanding Potential of Antennas, with Application to Cavity Backed Slots and Other Antennas," by A. Vassiliadis and R. L. Tanner, August 1960.

72. "A New Approach to the Evaluation of HF Aircraft Antennas," by J. F. Cline, March 1961.

73. "Precipitation Charging and Corona-Generated Interference in Aircraft," by R. L. Tanner and J. E. Nanevicz, May 1961.

74. "Transmission Through an Ionized Medium in the Presence of a Strong Magnetic Field," by H. S. Rothman and T. Morita.

STANFORD RESEARCH INSTITUTE

MENLO PARK
CALIFORNIA

Regional Offices and Laboratories

Southern California Laboratories
820 Mission Street
South Pasadena, California

Washington Office
808 17th Street, N.W.
Washington 6, D.C.

New York Office
270 Park Avenue, Room 1770
New York 17, New York

Detroit Office
1025 East Maple Road
Birmingham, Michigan

European Office
Pelikanstrasse 37
Zurich 1, Switzerland

Japan Office
911 Iino Building
22, 2-chome, Uchisaiwai-cho, Chiyoda-ku
Tokyo, Japan

Representatives

Honolulu, Hawaii
1125 Ala Moana Blvd.
Honolulu, Hawaii

London, England
19, Upper Brook Street
London, W. 1, England

Milan, Italy
Via Macedonio Melloni, 49
Milano, Italy

Toronto, Ontario, Canada
Room 710, 67 Yonge St.
Toronto, Ontario, Canada